BJR

https://doi.org/10.1259/bjr.20180476

Received: 27 May 2018 | Revised: 19 November 2018 | Accepted: 19 November 2018

Cite this article as:
Sosa Iglesias V, van Hoof SJ, Vaniqui A, Schyns LEJR, Lieuwes N, Yaromina A, et al. An orthotopic non-small cell lung cancer model for image-guided small animal radiotherapy platforms. *Br J Radiol* 2019; **92**: 20180476.

## SMALL ANIMAL IGRT SPECIAL FEATURE: FULL PAPER

# An orthotopic non-small cell lung cancer model for image-guided small animal radiotherapy platforms

**VENUS SOSA IGLESIAS, PhD, STEFAN J. VAN HOOF, MSc, ANA VANIQUI, MSc, LOTTE EJR SCHYNS, MSc, NATASJA LIEUWES, Ing, ALA YAROMINA, PhD, LINDA SPIEGELBERG, PhD, ARJAN J GROOT, PhD, FRANK VERHAEGEN, PhD, JAN THEYS, PhD, LUDWIG DUBOIS, PhD and MARC VOOIJS, PhD**

Department of Radiotherapy, GROW-School for Oncology & Developmental Biology, Maastricht University Medical Centre, Maastricht, The Netherlands

Address correspondence to:
Marc Vooijs
E-mail: *mvooys@gmail.com;marc.vooijs@maastrichtuniversity.nl*
Ludwig Dubois
E-mail: *ludwig.dubois@maastrichtuniversity.nl*

**Objective:** Lung cancer is the deadliest cancer worldwide. To increase treatment potential for lung cancer, pre-clinical models that allow testing and follow up of clinically relevant treatment modalities are essential. Therefore, we developed a single-nodule-based orthotopic non-small cell lung cancer tumor model which can be monitored using multimodal non-invasive imaging to select the optimal image-guided radiation treatment plan.

**Methods:** An orthotopic non-small cell lung cancer model in NMRI-nude mice was established to investigate the complementary information acquired from 80 kVp microcone-beam CT (micro-CBCT) and bioluminescence imaging (BLI) using different angles and filter settings. Different micro-CBCT-based radiation-delivery plans were evaluated based on their dose-volume histogram metrics of tumor and organs at risk to select the optimal treatment plan.

**Results:** H1299 cell suspensions injected directly into the lung render exponentially growing single tumor nodules whose CBCT-based volume quantification strongly correlated with BLI-integrated intensity. Parallel-opposed single angle beam plans through a single lung are preferred for smaller tumors, whereas for larger tumors, plans that spread the radiation dose across healthy tissues are favored.

**Conclusions:** Closely mimicking a clinical setting for lung cancer with highly advanced preclinical radiation treatment planning is possible in mice developing orthotopic lung tumors.

**Advances in knowledge:** BLI and CBCT imaging of orthotopic lung tumors provide complementary information in a temporal manner. The optimal radiotherapy plan is tumor volume-dependent.

## INTRODUCTION

Lung cancer remains the deadliest cancer worldwide whereby the non-small cell lung cancer (NSCLC) subtype accounts for ~85% of all lung cancers. Standard of care is a multimodal approach including surgery, radiotherapy, chemotherapy and targeted therapy, often administered in combination. Despite improvements in treatment techniques, overall survival has only marginally improved for advanced (Stage III–IV) lung cancer, and treatment cost has escalated.[1]

There is mounting evidence that the current pre–clinical mouse models for cancer treatment testing predict clinical response poorly. The most widely used models for anti-cancer drug testing are subcutaneous tumor xenografts. However, these models fail to recapitulate the interactions of the tumor with its microenvironment, which may influence response to chemotherapy[2] and radiotherapy.[3] Treatment resistance is partly due to a deficient tumor vasculature impeding normal blood flow and thus, both drug and nutrient delivery to the tumor.[4] Hence, a greater emphasis on reproducible and physiologically relevant preclinical tumor models is required to assess efficacy and toxicity of new interventions that target tumor progression and recurrence. Orthotopic tumor models are able to overcome, at least partially, this limitation. Orthotopically implanted NSCLC or spontaneous KRAS-induced lung tumors are thought to have better vasculature functionality.[5]

In addition, to improving cancer models that reflect advanced disease, quantitative non-invasive imaging modalities to monitor tumor progression and treatment

response dynamically in time such as the ones used in this study: CT and bioluminescence imaging (BLI), must be optimized. CT is suitable for longitudinal monitoring and accurate delineation of tumors for radiotherapy treatment planning.[6] Repeated—daily or multiple times per week for several weeks – use of CT should however be avoided because of the cumulative radiation dose to healthy tissues.[7] Studies using phantoms, and confirmed in small rodents, indicate that in order to increase precision, there must be an increase in the isotropic voxel size (thus decreasing image resolution) or an increase in the *X*-ray dose.[7] Recent improvements in detector technology have enabled enhanced resolution, however, high-quality images approach a lethal *X*-ray dose.[7] Therefore, image quality must be compromised to deliver doses as low as reasonably achievable to avoid bias in therapeutic efficacy and warrant animal welfare.[8] Additionally, tumor growth can be affected by doses greater than 1 Gy,[8] and depending on the sensitivity of the tumor, repeated CT scans could improve cancer morbidity by delaying tumor progression in certain tumor types.[9] BLI on the other hand, is a highly sensitive, non-invasive and radiation-free imaging modality that requires the expression of a luciferase enzyme to catalyze D-luciferin into oxyluciferin and light.[10,11] There is a gradual increase in tissue penetration at longer wavelengths and higher photon energies, potentially enabling insight on tumor depth.[12] However, light scattering, tissue penetration and absorption, makes absolute BLI quantification challenging.

Precision image-guided small animal radiotherapy (SmART) research platforms with an integrated cone beam CT (CBCT) scanner and BLI have become available which allows 1 mm precision sized beams for radiation delivery to minimize normal tissue toxicity.[13,14] We recently demonstrated that there was good correlation between micro-CT calculated tumor volume and BLI signal in a temporal manner for histopathologically confirmed intracranial brain tumors.[15] Radiation planning, using SmART-Plan software,[16] enables dose-volume calculations prior to delivery for design optimization and has been implemented for CT image-guided radiation planning of brain tumors to investigate combinations of conventional treatment regimens[17] and novel targeted drugs.[18] In this study we assessed this correlation for intrapulmonary NSCLC and investigated tumor volume-dependent differences in optimal radiation planning.

## METHODS AND MATERIALS

### Orthotopic tumor cell injection

NCI–H1299 and A549 NSCLC cells were cultured in DMEM medium whereas NCI-H460 was cultured in RPMI 1640 (Westburg) medium, supplemented with 10% fetal calf serum (Sigma–Aldrich). The origin of the cell lines is available at ATCC. To establish luciferase-expressing cells, H1299-GFP-luciferase[19] and A549–luc–C8[20] cells were generated as previously described. Cell line identity was confirmed by short-tandem repeat analysis (Identicell, Denmark) and tested for the presence of mycoplasma prior to their injection in 2536g NMRI-nude male mice (Charles River). Orthotopic implantation of tumor cells was performed as previously described but with modifications.[21] A small incision, parallel to the ribs, after the third "false rib" and the first "floating rib", was made and the muscles were carefully lifted using blunt scissors and considering muscle orientation to allow lung visualization through the rib cage and avoid lung collapse and pneumothorax. Specifically, $10^6$ tumor cells resuspended in 10–20 µL mixture (4:1) of Matrigel (Corning)—CT contrast agent (Omnipaque 350, GE Healthcare), were injected into the middle/upper lobe of the right lung, were movement is the least, using a 25G needle at a depth 6 mm (reference depth point: rib cage) between the seventh and eighth ribs (starting count in the first posterior "false rib") at maximal inhalation. Wound closure was obtained with 3M™ vetbond tissue adhesive (Bio-connect) and surgical suture. Pre-operative (Buprenorphine 0.1 mg $kg^{-1}$) and post-operative (Carprofen 5 mg $kg^{-1}$) analgesia were applied. At the end of the experiment, lungs were excised, formalin (4%)-fixed, paraffin-embedded, sectioned (5 µm), and stained with Hematoxylin and Eosin. Images were acquired with a phase contrast microscope at 10× magnification and stitched together for full visualization. Animal experiments were in accordance with local institutional guidelines for animal welfare and approved by the Animal Ethical Committee of the University of Maastricht.

### Micro-cone beam CT (CBCT) imaging and analysis

Multiple two-dimensional thoracic cone beam CT images (80 kVp, 3 mA, 120 s, 39cGy/scan) were acquired using an *X*-RAD 225Cx[22] small animal irradiator (Precision *X*-ray, Inc, North Branford, CT)[13,14,23] under isoflurane anesthesia. Image projections were reconstructed using the Feldkamp[24] filtered back projection (Pilot version 1.1.18; Precision *X*-ray, Inc), resulting in a three-dimensional isotropic pixel spacing of 102 µm. Pre-defined CT window settings of 1550 to −1480 Houndsfield Units (HU) for tumor and normal lung (total lung minus tumor), and of 250 to −150 HU for heart and spinal cord were used for structure delineations using in SmART-Plan.[16] Contours were exported as bitmasks after applying erosion with a spherical structuring element (1-pixel radius) to decrease inaccuracies of the contouring procedure. A three-dimensional bitmask was calculated from the two-dimensional contours using the poly2mask function in MATLAB R2016b (Mathworks, Natick, MA https://www.mathworks.com/help/images/ref/poly2mask.html). The voxels in the bitmask have the same size as the CT voxels therefore, the number of voxels in the tumor bitmask multiplied by the voxel size will result in the tumor volume. No spherical approximation formulas were used. Tumor volume ($Volume_{tumor}$) was calculated according to the formula: $Volume_{tumor}$ = (numberVoxels * voxelSpacingX * voxelSpacingY * voxelSpacingZ).

### Bioluminescence imaging

Under isoflurane anesthesia, whole-body white light and BLI scans from six angles (0, 90, 180, 225, 270, and 315 degrees corresponding to left, ventral, right, diagonal right, dorsal, and diagonal left sides respectively) were acquired with the iXon Ultra 897 camera (Andor Technology Ltd, Belfast, UK) in the *X*–RAD 225Cx using no (open modus), 591.5 or 655 nm filters 26 min after intraperitoneal injection of D-luciferin (300 µl solution, 15 mg $ml^{-1}$, in physiological saline).

Bioluminescence images were acquired with a gain of 300, an opacity at 70% and the signal intensity parameters were kept constant for all images ($W$ = 37977.48 and $L$ = 26438.27 for white light image, $W$ = 7767.0 and l = 5277.0 for BLI). The cumulative raw BLI intensity signal was corrected with the background signal corresponding to the average signal in the four corners of the image (30×30 pixels).

### Radiation treatment planning and dose calculation

Treatment plans based on parallel-opposed static, or two arc beams (with angles of 260–272° and 350–360°) using a 3 mm or a 5 mm circular collimator (SmART-Plan v1.5,[16]) for two different volumes were compared for mean ($D_{mean}$), minimum ($D_{min}$) and maximum ($D_{max}$) doses, dose to 95% ($D_{95}$), to 5% ($D_5$), and to 1% ($D_1$) of the delineated structure volume and the percentage of structure volume receiving 95% ($V_{95}$) of the prescribed dose. The beam angle with the best avoidance of organs at risk (OARs) was chosen. A 2-min-thoracic CBCT scan acquisition time enables imaging throughout the full respiratory cycle of the mouse (every 4 s under deep anesthesia), therefore the delineated tumor volume will be referred to as the internal target volume (ITV). Errors in planning, temporal tumor movement over the course of days, and treatment delivery uncertainties[16] were compensated with an additional 0.5 mm margin (planned target volume, PTV). Dose calculations were performed with the dose engine DOSXYZnrc (National Research Council Canada, Ottawa, ON) using an intrinsic dose uncertainty set to 1% in the target volume. The conversion of CT number to material type and density was performed based on a 3-material (air, soft tissue and bone) human tissue (International Commission on Radiation units and Measurements, report 44) segmentation scheme. A CT number-to-density calibration curve was established using a 3 cm diameter preclinical μCT calibration phantom with different tissue substitute inserts (SmART Scientific Solutions B.V., Maastricht, Netherlands). Dose calculations were run with $10^8$ particles for each treatment plan.

### Statistical analysis

Statistical analyses were performed using GraphPad Prism Software (v. 5.03). Normality distribution of tumor volume and bioluminescence data were assessed with a D'Agostino and Pearson omnibus test. Non-parametric Spearman correlation test was applied to determine the relationship between tumor volume by CBCT imaging and bioluminescence signal and further confirmed by linear regression analysis. A $p$-value < 0.05 was considered statistically significant.

## RESULTS

### Single orthotopic NSCLC nodules are feasible

Centrally localized tumors in the right lung were obtained after H1299 cell suspension injection (Figure 1A). Tumor location in the lung was macroscopically and histologically confirmed (Figure 1B) and tumor growth was exponential with an average doubling time of approximately 9 days (Figure 1C). H1299-luciferase expressing tumors (including a tumor with a centrally located calcification, D8) grew slower with a doubling time of approximately 19 days (Figure 1D), and occupying less than 7% of the right lung volume (or 5% of total lung volume, data not shown) after 80 days post-tumor cell implantation in the lung (Figure 1E). H460 and A549 cell suspension mixtures led to multiple lung nodules in the lung and thoracic cavity and experiments with these models were discontinued (data not shown). BLI signal intensity in H1299-luciferase expressing tumors increased with time and was most intense at the site of the tumor (Figure 2A, Supplementary Figure 1A–D in Supplementary Material 1). The BLI signal acquired from the 655 nm wavelength was 3-fold greater than that from the 591.5 nm wavelength and 12-fold less than the open modus (all wavelengths) (Fig 2A, Supplementary Figure 1A-D in Supplementary Material 1).

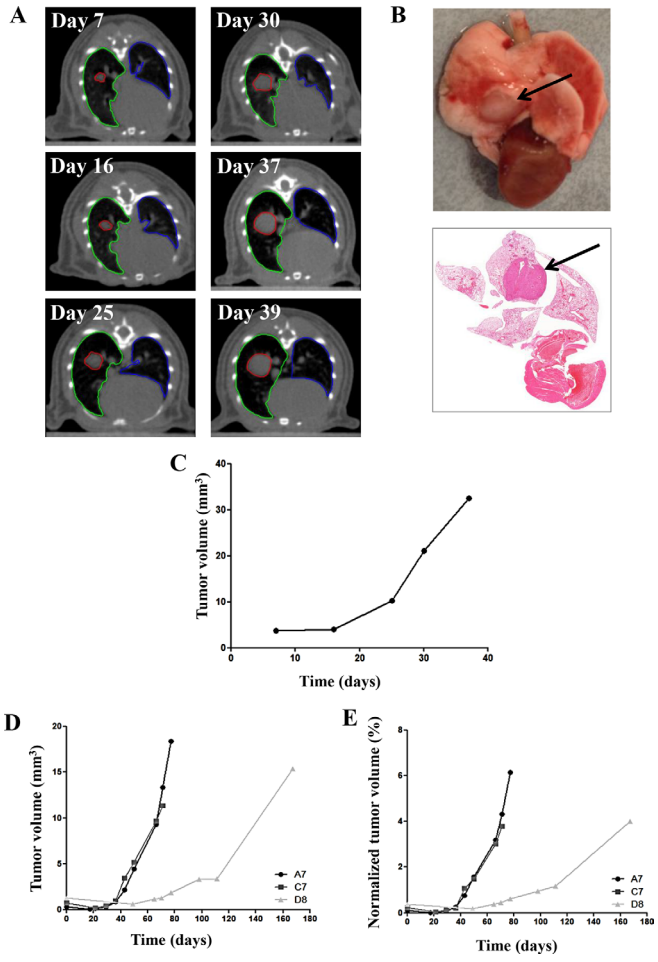


Figure 1. Establishment of single nodule orthotopic NSCLC models. (A) Representative 2D delineated CT images of selected time points after H1299 cell suspension injection in the right lung. Tumors, right and left lung are delineated in red, green and blue, respectively. (B) Macroscopic and histological confirmation of presence of a single tumor nodule in the right lung indicated with an arrow. (C) Tumor quantification over time of a representative orthotopic H1299-wildtype lung tumor. (D) Tumor quantification over time of three orthotopic H1299-luciferase lung tumors: A7, C7, and D8 (presenting a central calcification). (E) Normalized H1299-luciferase (from D) tumor volumes to total right lung volume quantification. NSCLC, non-small cell lung cancer.

Figure 2. Correlation between tumor volume determined by CBCT and BLI signal intensity over time. (A) Representative CBCT and 180-angle BLI images (overlaid on the white light image of the mouse) over time. (B) Correlation between CBCT-derived tumor volume ($mm^3$) and BLI intensity obtained from the 180-degree angle for three independent H1299-luciferase expressing tumors. CBCT, cone beam CT; BLI, bioluminescence imaging.

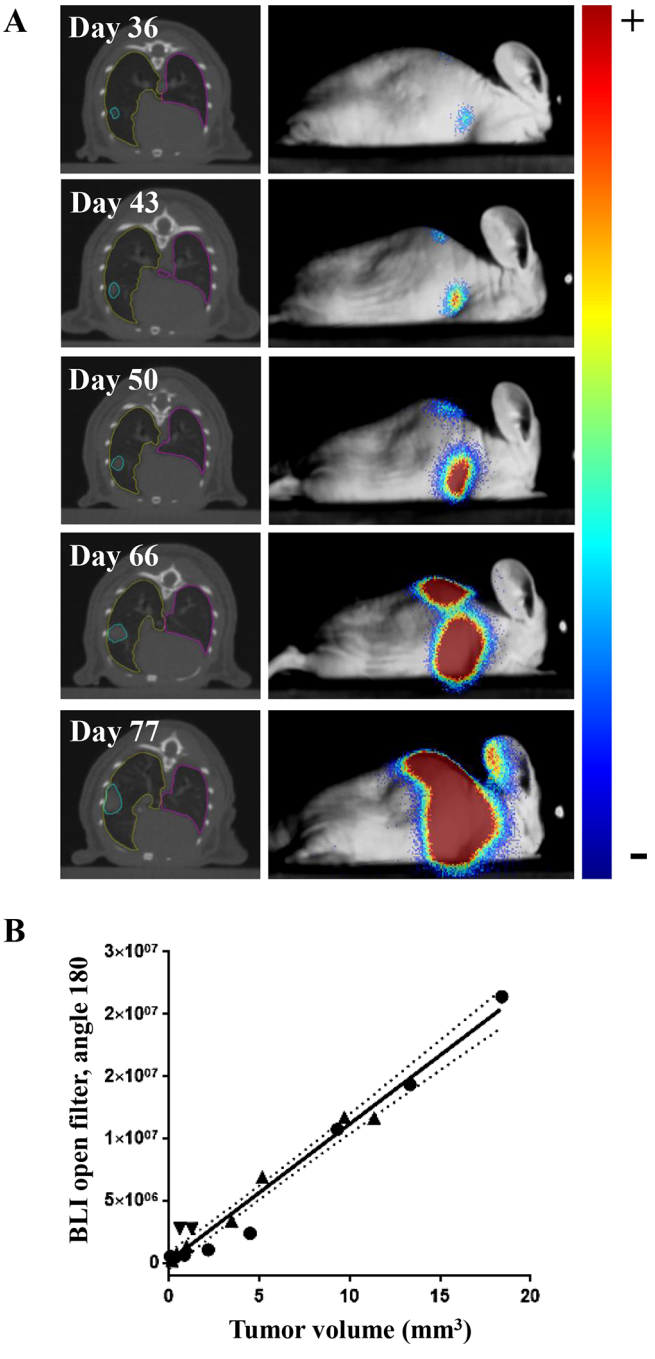


## CBCT volume and BLI signal intensity are correlated

Bioluminescent signals acquired with open modus correlated significantly ($r$ = 0.88 to 0.96, $p < 0.0001$) with tumor volume assessed by CBCT imaging (Figure 2B). Good correlations between CT and BLI were also observed for 655 nm ($r$ = 0.84–0.95, $p$-value < 0.001), and 591.5 nm ($r$ = 0.75–0.88, $p$-value < 0.05) filters (Supplementary Figure 1E in Supplementary Material 1). Similar results were obtained with $R^2$ linear regression fits (data not shown).

## Radiation treatment planning may be volume-dependent

Tumors and OAR (left lung, right lung, heart and spinal cord) were delineated on thoracic CT images of H1299-wt or H1299-luciferase tumor-bearing mice using SmART-plan software. Visual tumor coverage using different radiation beam plans (planned dose 2 Gy) with their corresponding dose–volume histograms (DVH) are shown for a 4 and 10.4 $mm^3$ H1299 tumor using a 3 (Figure 3A–B) or 5 mm (Figure 3C–D) collimator, respectively, and quantified in Tables 1 and 2, respectively (Supplementary tables 1 and 2, (Supplementary Material 1) for a planned dose of 20 Gy). The 3 and 5 mm collimator were optimal for a 4 (Table 1) and 10.4 $mm^3$ (Table 2) tumor respectively, irrespective of the tested plan, having a $D_{mean}$ within the PTV similar to the planned dose. The PTV $V_{95}$ was above 98.7%, independent of the tested volume, using the 5 mm collimator, whereas for the 3 mm collimator it ranged from 82.3 to 92.8% for a 4 $mm^3$ tumor. As expected, the $V_{95}$ for the 3 mm collimator for a 10.4 $mm^3$ tumor was inferior (58.2–76.9%). For a 3 mm collimator, a better PTV coverage can be obtained with parallel-opposed-based treatment plans from a single angle (Plan 1 and 2) compared to Plan 3 and 4, while for a 5 mm collimator each plan results in similar PTV coverage (Tables 1 and 2). Similar results were obtained for plans 1 and 2 using calcification-free H1299-luciferase expressing tumors A7 and C7 (Supplementary Table 3 in Supplementary Material 1). As expected, radiation plans on a calcified tumor (D8), were not as precise.

The optimal PTV coverage, however is associated with an increased volume of normal lung tissue receiving 95% of the delivered dose. Right lung $V_{95}$ was higher (up to 23.4% for the 3 mm and up to 35% for 5 mm collimator) in plans 1 and 2 compared to plans 3 and 4 (up to 4.5% for the 3 mm and up to 11% for 5 mm collimator). Remarkably, using a beam setup crossing both lungs (Plan 2), similar and only slightly reduced $V_{95}$ values were obtained for the left (Plan 2) and right (Plan 1) lung respectively. Despite covering both lungs, employing four equally weighted beams instead of two (as in plans 1 and 2) or the usage of two arc beams (Plan 4), greatly reduces the dose to the normal lung. Normal tissue mean radiation doses for heart and spinal cord were minor for any tested plan although the long-term dose-effects should be experimentally tested (Tables 1 and 2). Dose uniformity was found to be consistent across treatment plans (data not shown).

## DISCUSSION

In this study, we established an orthotopic NSCLC model and evaluated different radiation treatment plans using non-invasive image guidance. Not all NSCLC cell line models tested here resulted in a single localized tumor nodule in the lung. Others have reported that blind-percutaneous injection of H1299 cells into the left lateral thorax at 5–7 mm of depth, produced solitary

Figure 3. Volume-dependent radiation treatment planning. Representative beam setup in axial plane for four radiation plans: parallel-opposed, equally weighted single angle, static crossing a single lung (Plan 1), crossing both lungs (Plan 2), 2-angle parallel-opposed static (Plan 3), or two equally weighted arc (Plan 4) beams for a H1299 tumor model. Two tumors volumes are shown: volume 1 (4 $mm^3$) with the 3 mm collimator (A) and volume 2 (10.4 $mm^3$) with the 5 mm collimator (C), with their corresponding dose–volume histograms (B, D respectively). PTV, ITV, right lung, left lung, spinal cord and heart are indicated in green, light blue, yellow, pink, dark blue and red, respectively. ITV, internal target volume; PTV, planning targetvolume.

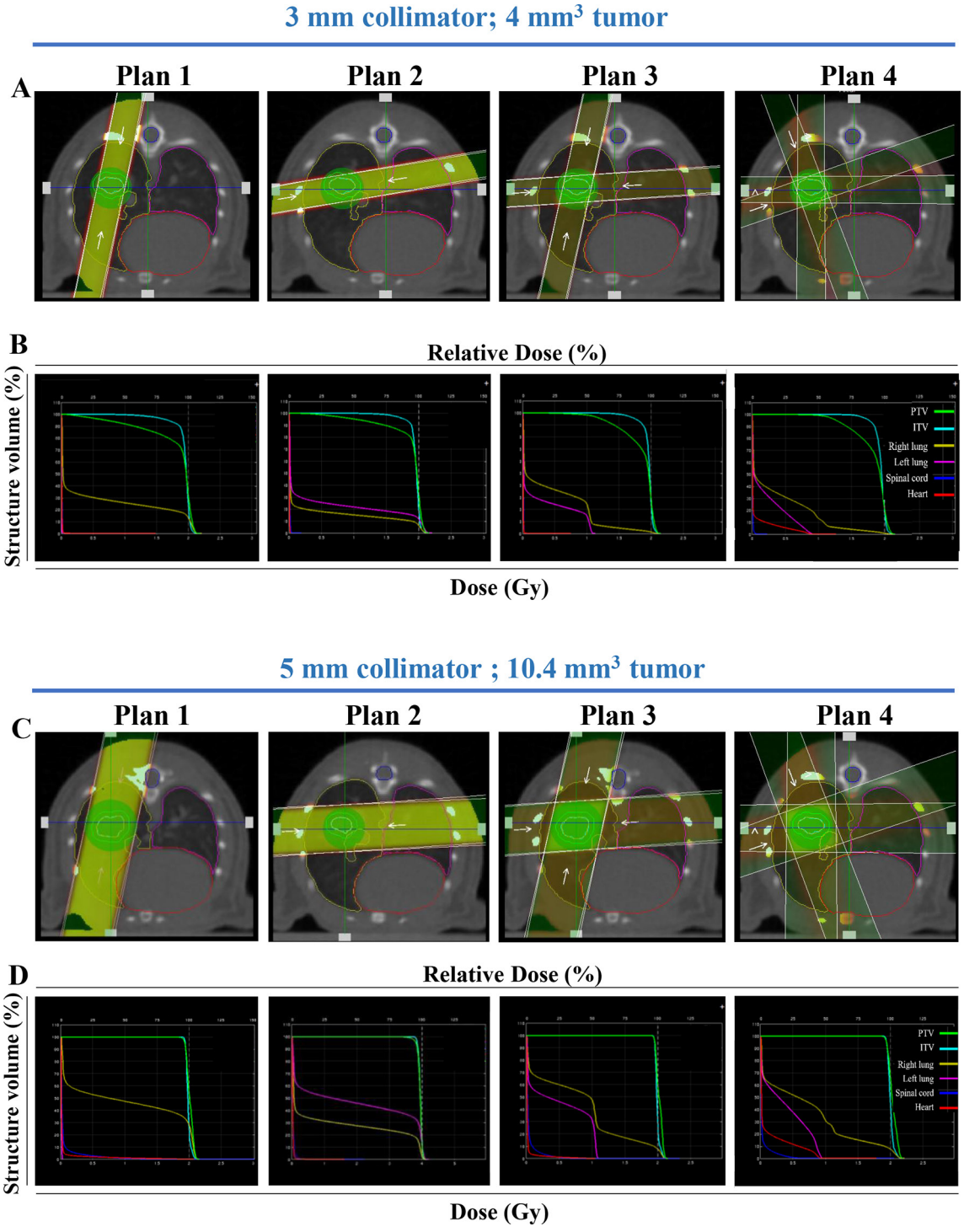


lesions that progressed into diffuse thoracic disease.[25] Mordant et al investigated the establishment of orthotopic lung tumors using the A549 cells and found that transpleural injections resulted in a 65% localized tumor take, followed by 7% locoregional invasion and 3% of bone metastasis.[26] Also, pleural injection of H460 cells has been shown to result in tumors in the lung and the chest wall with 100%

Table 1. Dose-volume histogram metrics for different structures (ITV, PTV, right/left lung, heart, spinal cord) for a representative mouse case bearing a H1299-wt tumor (4 $mm^3$) using four different radiation plans (see methodology), two collimators (3 mm and 5 mm), and a prescribed dose of 2 Gy

| Structure | Collimator | 3 mm | | | | 5 mm | | | |
|---|---|---|---|---|---|---|---|---|---|
| | Plan | 1 | 2 | 3 | 4 | 1 | 2 | 3 | 4 |
| ITV | Dmean (Gy) | 2.00 | 1.99 | 2.00 | 1.98 | 2.02 | 1.99 | 2.01 | 2.00 |
| | Dmin (Gy) | 1.57 | 1.72 | 1.78 | 1.77 | 1.94 | 1.91 | 1.92 | 1.91 |
| | Dmax (Gy) | 2.16 | 2.18 | 2.16 | 2.16 | 2.16 | 2.14 | 2.14 | 2.17 |
| | V95 (%) | 98.03 | 99.69 | 99.11 | 95.67 | 100.00 | 100.00 | 100.00 | 100.00 |
| | D95 (Gy) | 1.93 | 1.94 | 1.94 | 1.90 | 1.98 | 1.95 | 1.97 | 1.95 |
| | D5 (Gy) | 2.07 | 2.07 | 2.07 | 2.06 | 2.10 | 2.07 | 2.09 | 2.08 |
| | D1 (Gy) | 2.12 | 2.11 | 2.11 | 2.12 | 2.13 | 2.10 | 2.12 | 2.13 |
| PTV | Dmean (Gy) | 1.96 | 1.99 | 1.98 | 1.97 | 2.06 | 2.03 | 2.05 | 2.04 |
| | Dmin (Gy) | 0.00 | 0.00 | 0.00 | 0.00 | 0.00 | 0.00 | 0.00 | 0.00 |
| | Dmax (Gy) | 2.20 | 2.18 | 2.17 | 2.20 | 2.20 | 2.17 | 2.18 | 2.20 |
| | V95 (%) | 86.61 | 92.80 | 86.68 | 82.29 | 99.88 | 99.94 | 99.95 | 99.83 |
| | D95 (Gy) | 1.46 | 1.80 | 1.68 | 1.67 | 1.98 | 1.96 | 1.97 | 1.94 |
| | D5 (Gy) | 2.11 | 2.11 | 2.10 | 2.12 | 2.14 | 2.10 | 2.12 | 2.14 |
| | D1 (Gy) | 2.14 | 2.13 | 2.13 | 2.15 | 2.16 | 2.12 | 2.14 | 2.16 |
| Right lung | Dmean (Gy) | 0.73 | 0.35 | 0.54 | 0.51 | 1.22 | 0.61 | 0.91 | 0.87 |
| | Dmin (Gy) | 0.00 | 0.00 | 0.00 | 0.00 | 0.00 | 0.00 | 0.00 | 0.00 |
| | Dmax (Gy) | 2.21 | 2.20 | 2.17 | 2.22 | 2.22 | 2.17 | 2.18 | 2.24 |
| | V95 (%) | 24.55 | 11.20 | 4.54 | 4.20 | 47.73 | 21.74 | 15.15 | 14.50 |
| | D95 (Gy) | 0.01 | 0.00 | 0.01 | 0.01 | 0.02 | 0.01 | 0.02 | 0.02 |
| | D5 (Gy) | 2.10 | 2.04 | 1.84 | 1.82 | 2.13 | 2.08 | 2.08 | 2.09 |
| | D1 (Gy) | 2.13 | 2.10 | 2.07 | 2.08 | 2.16 | 2.11 | 2.11 | 2.15 |
| Left lung | Dmean (Gy) | 0.01 | 0.57 | 0.29 | 0.24 | 0.01 | 0.98 | 0.48 | 0.39 |
| | Dmin (Gy) | 0.00 | 0.00 | 0.00 | 0.00 | 0.00 | 0.00 | 0.00 | 0.00 |
| | Dmax (Gy) | 0.02 | 2.24 | 1.14 | 0.95 | 0.03 | 2.22 | 1.14 | 0.97 |
| | V95 (%) | 0.00 | 19.26 | 0.00 | 0.00 | 0.00 | 36.68 | 0.00 | 0.00 |
| | D95 (Gy) | 0.00 | 0.01 | 0.01 | 0.01 | 0.00 | 0.02 | 0.01 | 0.01 |
| | D5 (Gy) | 0.01 | 2.11 | 1.06 | 0.77 | 0.02 | 2.13 | 1.08 | 0.86 |
| | D1 (Gy) | 0.01 | 2.16 | 1.09 | 0.86 | 0.02 | 2.15 | 1.10 | 0.91 |
| Heart | Dmean (Gy) | 0.01 | 0.01 | 0.01 | 0.02 | 0.02 | 0.02 | 0.02 | 0.07 |
| | Dmin (Gy) | 0.00 | 0.00 | 0.00 | 0.00 | 0.00 | 0.00 | 0.00 | 0.00 |
| | Dmax (Gy) | 0.11 | 0.13 | 0.09 | 0.69 | 1.82 | 1.79 | 0.93 | 0.94 |
| | V95 (%) | 0.00 | 0.00 | 0.00 | 0.00 | 0.00 | 0.00 | 0.00 | 0.00 |
| | D95 (Gy) | 0.00 | 0.00 | 0.00 | 0.00 | 0.01 | 0.01 | 0.01 | 0.01 |
| | D5 (Gy) | 0.02 | 0.02 | 0.02 | 0.11 | 0.04 | 0.04 | 0.04 | 0.42 |
| | D1 (Gy) | 0.02 | 0.02 | 0.02 | 0.41 | 0.31 | 0.11 | 0.27 | 0.72 |

(Continued)

Table 1. (Continued)

| Structure | Collimator | 3 mm | | | | 5 mm | | | |
|---|---|---|---|---|---|---|---|---|---|
| | Plan | 1 | 2 | 3 | 4 | 1 | 2 | 3 | 4 |
| Spinal cord | Dmean (Gy) | 0.01 | 0.01 | 0.01 | 0.01 | 0.04 | 0.11 | 0.06 | 0.06 |
| | Dmin (Gy) | 0.00 | 0.00 | 0.00 | 0.00 | 0.01 | 0.00 | 0.00 | 0.00 |
| | Dmax (Gy) | 0.07 | 0.51 | 0.24 | 0.31 | 0.88 | 1.94 | 1.01 | 0.85 |
| | V95 (%) | 0.00 | 0.00 | 0.00 | 0.00 | 0.00 | 0.06 | 0.00 | 0.00 |
| | D95 (Gy) | 0.00 | 0.00 | 0.00 | 0.00 | 0.01 | 0.00 | 0.01 | 0.01 |
| | D5 (Gy) | 0.02 | 0.03 | 0.02 | 0.02 | 0.08 | 0.69 | 0.30 | 0.33 |
| | D1 (Gy) | 0.03 | 0.06 | 0.04 | 0.07 | 0.38 | 1.61 | 0.83 | 0.67 |

Dmax, maximum PTV dose (Gy); $D_{mean}$, mean PTV dose (Gy); $D_{min}$, minimum PTV dose (Gy); ITV, internal target volume; PTV, planned target volume; V95, Percentage (%) of PTV receiving 95% of the prescribed dose.
Dmean: Mean PTV dose (Gy),Dmin: Minimum PTV dose (Gy), Dmax: Maximum PTV dose (Gy), V95: Percentage (%) of PTV receiving 95% of the prescribed dose, and D95, D5, D1 are the doses to the hottest 95%, 5%, or1% delineated structure.

occurrence of mediastinal nodal metastasis, and death after 19 days.[27] One of the tumors (D8) in this study presented a centrally located bone-like dense structure (possibly a calcification), which not only delayed H1299-luciferase tumor growth considerably, but also affected the DVH metrics in radiation planning. In the clinic, this event occurs in 10.6% of lung carcinomas,[28] therefore optimal radiation treatment strategies are needed.

We have shown that tumor growth in the mouse lung can be monitored over time using two non-invasive imaging modalities (CBCT and BLI), and can provide quantitative or semi-quantitative temporal information on tumor volume, respectively. Our data on orthotopic lung tumors are in line with our previous data and that of others, on orthotopic brain tumors, where correlation between CBCT and BLI have been reported in context of radiotherapy combination treatments.[15,17,18,29,30] For orthotopic lung tumor models, Madero et al has shown that BLI signal from A549 tumors had a strong correlation with the histologically determined tumor burden.[31] It has also been observed in orthotopic mouse LLC tumors that 80kV micro-CT tumor volume is correlated with BLI intensity.[21] These data are in line with our study and we extended these findings using human cell lines by showing that CT and BLI correlate, in both the open modus as well as using selective wavelength filters (655 and 591.5 nm). This addition can set a base for further research and algorithm development to obtain spatial information from BLI data. Other studies have also reported correlation between imaging techniques in orthotopic lung tumors:[19] -FDG-PET imaging and BLI with A549 tumors[32] and MRI using gadolinium-nanoparticles, and BLI with H358-Luciferase tumors.[33]

Using a preclinical orthotopic NSCLC model, we demonstrated the feasibility of image-guided radiotherapy using a small animal irradiator. Deviations due to respiration can lead to an overestimation of the mean tumor dose of up to 11% as assessed with 4D-MOBY phantoms,[34] but these deviations were avoided by acquiring images in a 2 min time frame, similar to a "slow" CBCT scan in the clinic. Gating for respiratory motion was not applied in this study and remains understudied preclinically. In the clinic, a 5 mm clinical target volume margin[35] is applied. Given that the tumors we worked with in this study have a smooth surface, localized position, and errors due to breathing motion are accounted for by doing a slow (in relation to the breathing frequency of the mouse) CBCT scan, we suggested a PTV margin of 0.5 mm to take into account the error associated with a difference in voxel size. Delineations of the tumor and OAR were done using pre-defined window settings, slightly broader than previously described.[36] Because the measured volume of tumors in the lung is highly dependent on the window width and level used during analysis as has been previously reported,[35] these parameters were kept constant in our study. Furthermore, we acquired BLI emission at different wavelengths. It has been recently described that the tissue penetrance of the 655 nm wavelength is ~2 mm and that of the 591.5 nm is of ~1 mm using low-level laser therapy in human skin.[37] Our results suggest that given the difference in signal intensity between wavelengths, algorithms could be developed to determine the spatial location of tumors. Such advances would be necessary to further the use of BLI as an alternative modality to CBCT for radiation-treatment planning.

Four different treatment plan setups with two different collimators for two different tumor sizes were investigated to define the optimal treatment plan (maximum homogeneous dose to the tumor and minimum dose to OAR). We observed that the 5 mm collimator gives the best tumor coverage for both volumes but comes with an enhanced dose to healthy lung for smaller tumors. Our results indicate that parallel-opposed static beams give a better tumor coverage for the 3 mm collimator while there was no difference for a 5 mm collimator. This is in line with our previous results for orthotopic brain tumors using two static parallel-opposed beams.[17] Parallel-opposed single–angle beams through one lung are advised since there is only a slight reduction in $V_{95}$ for PTV compared to plans that cross-both lungs, but there is less dose to the healthy lung. However, because there may be changes in normal tissues throughout the course of radiotherapy, it has been advised to complement the DVH metric analysis with biomarkers or imaging features in predictive model calculations.[38] For a smaller tumor, we recommend to use a 3 mm collimator and a parallel-opposed

Table 2. Dose–volume histogram metrics for different structures (ITV, PTV, right/left lung, heart, spinal cord) for a representative mouse case bearing a H1299-wt tumor (10.4 $mm^3$) using four different radiation plans (see methodology), two collimators (3 mm and 5 mm), and a prescribed dose of 2 Gy

| Structure | Collimator | 3 mm | | | | 5 mm | | | |
|---|---|---|---|---|---|---|---|---|---|
| | Plan | 1 | 2 | 3 | 4 | 1 | 2 | 3 | 4 |
| ITV | Dmean (Gy) | 1.94 | 1.95 | 1.95 | 1.94 | 1.98 | 1.99 | 1.99 | 2.00 |
| | Dmin (Gy) | 0.58 | 0.73 | 0.90 | 1.20 | 1.88 | 1.89 | 1.90 | 1.90 |
| | Dmax (Gy) | 2.14 | 2.15 | 2.15 | 2.16 | 2.15 | 2.15 | 2.14 | 2.18 |
| | V95 (%) | 85.34 | 87.28 | 87.6 | 79.13 | 99.87 | 99.98 | 99.99 | 99.91 |
| | D95 (Gy) | 1.68 | 1.78 | 1.76 | 1.77 | 1.94 | 1.94 | 1.95 | 1.94 |
| | D5 (Gy) | 2.04 | 2.03 | 2.04 | 2.03 | 2.06 | 2.06 | 2.06 | 2.08 |
| | D1 (Gy) | 2.08 | 2.08 | 2.09 | 2.09 | 2.09 | 2.09 | 2.09 | 2.13 |
| PTV | Dmean (Gy) | 1.79 | 1.86 | 1.84 | 1.83 | 2.01 | 2.02 | 2.02 | 2.03 |
| | Dmin (Gy) | 0.04 | 0.07 | 0.17 | 0.48 | 1.69 | 1.88 | 1.84 | 1.77 |
| | Dmax (Gy) | 2.19 | 2.16 | 2.15 | 2.16 | 2.16 | 2.17 | 2.16 | 2.20 |
| | V95 (%) | 69.83 | 76.85 | 65.81 | 58.17 | 98.66 | 99.98 | 99.88 | 99.45 |
| | D95 (Gy) | 0.71 | 1.02 | 1.23 | 1.27 | 1.93 | 1.95 | 1.95 | 1.94 |
| | D5 (Gy) | 2.08 | 2.07 | 2.07 | 2.07 | 2.09 | 2.10 | 2.09 | 2.14 |
| | D1 (Gy) | 2.12 | 2.10 | 2.10 | 2.11 | 2.11 | 2.12 | 2.11 | 2.16 |
| Right lung | Dmean (Gy) | 0.54 | 0.32 | 0.43 | 0.37 | 0.98 | 0.61 | 0.80 | 0.69 |
| | Dmin (Gy) | 0.00 | 0.00 | 0.00 | 0.00 | 0.00 | 0.00 | 0.00 | 0.00 |
| | Dmax (Gy) | 2.21 | 2.20 | 2.15 | 2.16 | 2.18 | 2.17 | 2.18 | 2.22 |
| | V95 (%) | 17.68 | 9.89 | 2.25 | 1.80 | 34.98 | 21.00 | 10.96 | 10.14 |
| | D95 (Gy) | 0.01 | 0.00 | 0.01 | 0.01 | 0.02 | 0.01 | 0.02 | 0.01 |
| | D5 (Gy) | 2.07 | 2.02 | 1.44 | 1.36 | 2.08 | 2.08 | 2.04 | 2.05 |
| | D1 (Gy) | 2.11 | 2.08 | 2.02 | 1.99 | 2.11 | 2.10 | 2.09 | 2.13 |
| Left lung | Dmean (Gy) | 0.01 | 0.47 | 0.26 | 0.20 | 0.01 | 0.97 | 0.49 | 0.37 |
| | Dmin (Gy) | 0.00 | 0.00 | 0.00 | 0.00 | 0.00 | 0.00 | 0.00 | 0.00 |
| | Dmax (Gy) | 0.02 | 2.21 | 1.14 | 0.97 | 0.04 | 2.20 | 1.12 | 1.00 |
| | V95 (%) | 0.00 | 15.03 | 0.00 | 0.00 | 0.00 | 35.06 | 0.00 | 0.00 |
| | D95 (Gy) | 0.00 | 0.01 | 0.00 | 0.00 | 0.01 | 0.02 | 0.01 | 0.01 |
| | D5 (Gy) | 0.01 | 2.07 | 1.05 | 0.79 | 0.02 | 2.12 | 1.07 | 0.90 |
| | D1 (Gy) | 0.01 | 2.13 | 1.08 | 0.89 | 0.03 | 2.14 | 1.08 | 0.94 |
| Heart | Dmean (Gy) | 0.01 | 0.01 | 0.01 | 0.07 | 0.04 | 0.02 | 0.03 | 0.13 |
| | Dmin (Gy) | 0.00 | 0.00 | 0.00 | 0.00 | 0.00 | 0.00 | 0.00 | 0.00 |
| | Dmax (Gy) | 1.49 | 0.03 | 0.75 | 1.27 | 2.07 | 1.08 | 1.05 | 1.78 |
| | V95 (%) | 0.00 | 0.00 | 0.00 | 0.00 | 0.11 | 0.00 | 0.00 | 0.00 |
| | D95 (Gy) | 0.00 | 0.00 | 0.00 | 0.00 | 0.01 | 0.01 | 0.01 | 0.01 |
| | D5 (Gy) | 0.02 | 0.01 | 0.02 | 0.54 | 0.05 | 0.04 | 0.05 | 0.82 |
| | D1 (Gy) | 0.03 | 0.02 | 0.02 | 0.84 | 1.17 | 0.06 | 0.59 | 0.90 |

(Continued)

Table 2. (Continued)

| Structure | Collimator | 3 mm | | | | 5 mm | | | |
|---|---|---|---|---|---|---|---|---|---|
| | Plan | 1 | 2 | 3 | 4 | 1 | 2 | 3 | 4 |
| Spinal cord | Dmean (Gy) | 0.01 | 0.01 | 0.01 | 0.01 | 0.06 | 0.03 | 0.05 | 0.04 |
| | Dmin (Gy) | 0.00 | 0.00 | 0.00 | 0.00 | 0.00 | 0.00 | 0.00 | 0.00 |
| | Dmax (Gy) | 0.19 | 0.19 | 0.11 | 0.23 | 4.46 | 2.88 | 2.33 | 2.06 |
| | V95 (%) | 0.00 | 0.00 | 0.00 | 0.00 | 0.06 | 0.01 | 0.01 | 0.00 |
| | D95 (Gy) | 0.00 | 0.00 | 0.00 | 0.00 | 0.01 | 0.00 | 0.01 | 0.00 |
| | D5 (Gy) | 0.02 | 0.02 | 0.02 | 0.02 | 0.24 | 0.09 | 0.21 | 0.21 |
| | D1 (Gy) | 0.03 | 0.03 | 0.02 | 0.04 | 0.92 | 0.40 | 0.50 | 0.47 |

Dmax, maximum PTV dose (Gy); Dmin, minimum PTV dose (Gy); V95, percentage (%) of PTVreceiving 95% of the prescribed dose, and D95, D5, D1 are the doses to the hottest 95%, 5%, or 1% delineated structure.
Dmean: Mean PTV dose (Gy),Dmin: Minimum PTV dose (Gy), Dmax: Maximum PTV dose (Gy), V95: Percentage (%) of PTV receiving 95% of the prescribed dose, and D95, D5, D1 are the doses to the hottest 95%, 5%, or 1% delineated structure.

single-angle treatment plan crossing a single lung. For larger orthotopic lung tumors, a 5 mm collimator is preferred using a beam plan that spreads the dose to the healthy tissue (parallel-opposed multi angle or arc treatment).

In conclusion, BLI and CBCT of orthotopic lung tumors provide complementary information regarding tumor growth. CBCT is preferably used for radiotherapy treatment planning, while BLI for monitoring tumor progression and treatment response. The optimal treatment plan, taking into account highest tumor coverage and lowest dose deposition in healthy tissue, may depend on tumor volume.

## ACKNOWLEDGEMENTS

This work was supported by World-Wide Cancer research (AICR 1311–97) and European Research Council, H2020 ERC-Consolidator grant (#617060).

## COMPETING INTERESTS

There are no competing interests

## ETHICS APPROVAL

**Protocol # 2014-051** Establishment of a single localized orthotopic lung tumor in mice and tumor growth monitoring with microCT.

## REFERENCES

1. Roth JA, Goulart BH, Ravelo A, Kolkey H, Ramsey SD. Survival gains from first-line systemic therapy in metastatic non-small cell lung cancer in the US., 1990–2015: Progress and opportunities. *Oncologist* 2017; **22**: 304–10. doi: https://doi.org/10.1634/theoncologist.2016-0253
2. Trédan O, Galmarini CM, Patel K, Tannock IF. Drug resistance and the solid tumor microenvironment. *J Natl Cancer Inst* 2007; **99**: 1441–54. doi: https://doi.org/10.1093/jnci/djm135
3. Barker HE, Paget JT, Khan AA, Harrington KJ. The tumour microenvironment after radiotherapy: Mechanisms of resistance and recurrence. *Nat Rev Cancer* 2015; **15**: 409–25. doi: https://doi.org/10.1038/nrc3958
4. Graves EE, Maity A, Le QT, . The tumor microenvironment in non-small-cell lung cancer. *Semin Radiat Oncol* 2010; **20**: 156–63. doi: https://doi.org/10.1016/j.semradonc.2010.01.003
5. Vilalta M, Hughes NP, Von Eyben R, Giaccia AJ, Graves EE. Patterns of vasculature in mouse models of lung cancer are dependent on location. *Mol Imaging Biol* 2017; **19**: 215–24. doi: https://doi.org/10.1007/s11307-016-1010-5
6. Lindsay PE, Granton PV, Gasparini A, Jelveh S, Clarkson R, van Hoof S, et al. Multi-institutional dosimetric and geometric commissioning of image-guided small animal irradiators. *Med Phys* 2014; **41**: 031714. doi: https://doi.org/10.1118/1.4866215
7. Ford NL, Thornton MM, Holdsworth DW. Fundamental image quality limits for microcomputed tomography in small animals. *Med Phys* 2003; **30**: 2869–77. doi: https://doi.org/10.1118/1.1617353
8. Workman P, Aboagye EO, Balkwill F, Balmain A, Bruder G, Chaplin DJ, et al. Guidelines for the welfare and use of animals in cancer research. *Br J Cancer* 2010; **102**: 1555–77. doi: https://doi.org/10.1038/sj.bjc.6605642
9. Lemon JA, Phan N, Boreham DR. Multiple CT scans extend lifespan by delaying cancer progression in cancer-prone mice. *Radiat Res* 2017; **188**: 495–504. doi: https://doi.org/10.1667/RR14575.1
10. Vooijs M, Jonkers J, Lyons S, Berns A. Noninvasive imaging of spontaneous retinoblastoma pathway-dependent tumors in mice. *Cancer Res* 2002; **62**: 1862–7.
11. Dubois LJ, Verhaegen F, Vooijs MA. Secreted reporter proteins, a valuable complementary tool for non-invasive preclinical monitoring of brain tumour growth. *Transl Cancer Res* 2016; **5**: S1486–S1488. doi: https://doi.org/10.21037/tcr.2016.12.52
12. Rice BW, Cable MD, Nelson MB. In vivo imaging of light-emitting probes. *J Biomed Opt* 2001; **6**: 432–40. doi: https://doi.org/10.1117/1.1413210
13. Verhaegen F, Granton P, Tryggestad E. Small animal radiotherapy research

platforms. *Phys Med Biol* 2011; **56**: R55–R83. doi: https://doi.org/10.1088/0031-9155/56/12/R01
14. Prise KM, Verhaegen F. Small animal image-guided radiotherapy. *Br J Radiol* 2017; **90**: 20160905. doi: https://doi.org/10.1259/bjr.20160905
15. Yahyanejad S, Granton PV, Lieuwes NG, Gilmour L, Dubois L, Theys J, et al. Complementary use of Bioluminescence Imaging and Contrast-Enhanced Micro—Computed Tomography in an Orthotopic Brain Tumor model. *Mol Imaging* 2014; **13**: 1–8. doi: https://doi.org/10.2310/7290.2014.00038
16. van Hoof SJ, Granton PV, Verhaegen F. Development and validation of a treatment planning system for small animal radiotherapy: SmART-Plan. *Radiother Oncol* 2013; **109**: 361–6. doi: https://doi.org/10.1016/j.radonc.2013.10.003
17. Yahyanejad S, van Hoof SJ, Theys J, Barbeau LM, Granton PV, Paesmans K, et al. An image guided small animal radiation therapy platform (SmART) to monitor glioblastoma progression and therapy response. *Radiother Oncol* 2015; **116**: 467–72. doi: https://doi.org/10.1016/j.radonc.2015.06.020
18. Yahyanejad S, King H, Iglesias VS, Granton PV, Barbeau LM, van Hoof SJ, et al. NOTCH blockade combined with radiation therapy and temozolomide prolongs survival of orthotopic glioblastoma. *Oncotarget* 2016; **7**: 41251–64. doi: https://doi.org/10.18632/oncotarget.9275
19. Konings GF, Cornel KM, Xanthoulea S, Delvoux B, Skowron MA, Kooreman L, et al. Blocking 17β-hydroxysteroid dehydrogenase type 1 in endometrial cancer: a potential novel endocrine therapeutic approach. *J Pathol* 2018; **244**: 203–14. doi: https://doi.org/10.1002/path.5004
20. Jenkins DE, Oei Y, Hornig YS, Yu SF, Dusich J, Purchio T, et al. Bioluminescent imaging (BLI) to improve and refine traditional murine models of tumor growth and metastasis. *Clin Exp Metastasis* 2003; **20**: 733–44. doi: https://doi.org/10.1023/B:CLIN.0000006815.49932.98
21. Fushiki H, Kanoh-Azuma T, Katoh M, Kawabata K, Jiang J, Tsuchiya N, et al. Quantification of mouse pulmonary cancer models by microcomputed tomography imaging. *Cancer Sci* 2009; **100**: 1544–9. doi: https://doi.org/10.1111/j.1349-7006.2009.01199.x
22. Clarkson R, Lindsay PE, Ansell S, Wilson G, Jelveh S, Hill RP, et al. Characterization of image quality and image-guidance performance of a preclinical microirradiator. *Med Phys* 2011; **38**: 845–56. doi: https://doi.org/10.1118/1.3533947
23. Verhaegen F, van Hoof S, Granton PV, Trani D. A review of treatment planning for precision image-guided photon beam pre-clinical animal radiation studies. *Z Med Phys* 2014; **24**: 323–34. doi: https://doi.org/10.1016/j.zemedi.2014.02.004
24. Feldkamp LA, Davis LC, Kress JW. Practical cone-beam algorithm. *J Opt Soc Amer A* 1984; **1**: 612–9. doi: https://doi.org/10.1364/JOSAA.1.000612
25. Onn A, Isobe T, Itasaka S, Wu W, O'Reilly MS, Ki Hong W, et al. Development of an orthotopic model to study the biology and therapy of primary human lung cancer in nude mice. *Clin Cancer Res* 2003; **9**: 5532–9.
26. Mordant P, Loriot Y, Lahon B, Castier Y, Lesèche G, Soria JC, et al. Bioluminescent orthotopic mouse models of human localized non-small cell lung cancer: feasibility and identification of circulating tumour cells. *PLoS One* 2011; **6**: e26073. doi: https://doi.org/10.1371/journal.pone.0026073
27. Takahashi O, Komaki R, Smith PD, Jürgensmeier JM, Ryan A, Bekele BN, et al. Combined MEK and VEGFR inhibition in orthotopic human lung cancer models results in enhanced inhibition of tumor angiogenesis, growth, and metastasis. *Clin Cancer Res* 2012; **18**: 1641–54. doi: https://doi.org/10.1158/1078-0432.CCR-11-2324
28. Grewal RG, Austin JH. CT demonstration of calcification in carcinoma of the lung. *J Comput Assist Tomogr* 1994; **18**: 867–71. doi: https://doi.org/10.1097/00004728-199411000-00004
29. Kirschner S, Felix MC, Hartmann L, Bierbaum M, Maros ME, Kerl HU, et al. *In vivo* micro-CT imaging of untreated and irradiated orthotopic glioblastoma xenografts in mice: capabilities, limitations and a comparison with bioluminescence imaging. *J Neurooncol* 2015; **122**: 245–54. doi: https://doi.org/10.1007/s11060-014-1708-7
30. Granton PV, Yahyanejad S, Vooijs MA. SmART-ER imaging and treatment of glioblastoma. *J Neurooncol* 2015; **123**: 319–20. doi: https://doi.org/10.1007/s11060-015-1801-6
31. Madero-Visbal RA, Colon JF, Hernandez IC, Limaye A, Smith J, Lee CM, et al. Bioluminescence imaging correlates with tumor progression in an orthotopic mouse model of lung cancer. *Surg Oncol* 2012; **21**: 23–9. doi: https://doi.org/10.1016/j.suronc.2010.07.008
32. Peng L, Feng L, Yuan H, Benhabbour SR, Mumper RJ. Development of a novel orthotopic non-small cell lung cancer model and therapeutic benefit of 2'-(2-bromohexadecanoyl)-docetaxel conjugate nanoparticles. *Nanomedicine* 2014; **10**: 1497–506. doi: https://doi.org/10.1016/j.nano.2014.03.016
33. Bianchi A, Dufort S, Lux F, Fortin PY, Tassali N, Tillement O, et al. Targeting and *in vivo* imaging of non-small-cell lung cancer using nebulized multimodal contrast agents. *Proc Natl Acad Sci U S A* 2014; **111**: 9247–52. doi: https://doi.org/10.1073/pnas.1402196111
34. van der Heyden B, van Hoof SJ, Schyns LE, Verhaegen F. The influence of respiratory motion on dose delivery in a mouse lung tumour irradiation using the 4D MOBY phantom. *Br J Radiol* 2017; **90**: 20160419. doi: https://doi.org/10.1259/bjr.20160419
35. De Ruysscher D, Faivre-Finn C, Nestle U, Hurkmans CW, Le Péchoux C, Price A, et al. European organisation for research and treatment of cancer recommendations for planning and delivery of high-dose, high-precision radiotherapy for lung cancer. *J Clin Oncol* 2010; **28**: 5301–10. doi: https://doi.org/10.1200/JCO.2010.30.3271
36. Harris KM, Adams H, Lloyd DC, Harvey DJ. The effect on apparent size of simulated pulmonary nodules of using three standard CT window settings. *Clin Radiol* 1993; **47**: 241–4. doi: https://doi.org/10.1016/S0009-9260(05)81130-4
37. Avci P, Gupta GK, Clark J, Wikonkal N, Hamblin MR. Low-level laser (light) therapy (LLLT) for treatment of hair loss. *Lasers Surg Med* 2014; **46**: 144–51. doi: https://doi.org/10.1002/lsm.22170
38. Bentzen SM, Parliament M, Deasy JO, Dicker A, Curran WJ, Williams JP, et al. Biomarkers and surrogate endpoints for normal-tissue effects of radiation therapy: The importance of dose-volume effects. *Int J Radiat Oncol Biol Phys* 2010; **76**: S145–S150. doi: https://doi.org/10.1016/j.ijrobp.2009.08.076